DOI 10.24425/aee.2025.154986

Effects of additional magnets and iron components in the rotor on flux control of a hybrid-excited synchronous machine

PIOTR PAPLICKI ✉, RYSZARD PALKA

West Pomeranian University of Technology, Department of Electrical Machines and Drives
ul. Sikorskiego 37, 70-313 Szczecin, Poland
e-mail: {✉ paplicki/rpalka}@zut.edu.pl

(Received: 30.08.2024, revised: 16.08.2025)

Abstract: Hybrid excitation in electrical machines is a technology that combines the advantages of field windings and permanent magnets for exciting magnetic flux. Hybrid excitation with controllable flux gives specific benefits that can be used in applications, such as electric vehicle motors and wind power generators. The paper presents an analysis of the influence of additional magnets and iron components embedded in rotor geometry on magnetic flux control of the Electric Controlled Permanent Magnet Synchronous machine (ECPMS-machine). 3D-finite element analyses of no-load magnetic flux density distribution, magnetic flux linkage, back electromotive force (BEMF) characteristics performed at different field windings conditions of the machine in three rotor design cases have been carried out and discussed. Experimental verification on the machine prototype with a selected case of the rotor design has been performed.

Key words: 3D-FEA, DC field-control, electrical machines, experimental validation, hybrid excitation, permanent magnet

1. Introduction

Over the last twenty years, many papers have been published relating to the problem of excitation flux control of permanent magnet (PM) machines, especially operating in a wide speed range. This issue is especially important in electric vehicle motors where the efficiency of a motor (often expressed by an efficiency map) is related to the speed and torque. In general, despite significant technological and scientific progress in the electric machines' modern structures, PM machines have some specified regions on the efficiency map with high efficiency, and in other regions the efficiency is much lower. Hence, the expansion of the area of high efficiency of PM machines and effective flux control techniques are still expected.

A special class within synchronous machines are hybrid excited (HE) (subsequently, the same abbreviation "HE" is sometimes employed to signify "hybrid excitation.") machines with two sources of magnetic flux excitation. The purpose of a combination of these two sources is to combine the advantage of PM machines with those of electrically excited synchronous machines. The main advantage of HE machines is that their flux is variable. This is in contrast to typical PM machines, where the flux excited by PM cannot be controlled. The variable flux can change the voltage level of the induced electromotive force (EMF), making it controllable, and can increase the torque at low speeds. Moreover, hybrid excitation constitutes an additional degree of freedom in machine design flexibility. The effective performance of HE machines, in terms of operational flexibility at high speeds and their optimized efficiency, especially in motoring mode of the machine, has received growing attention in recent years [1–12]. Moreover, in generating mode, HE machines are an interesting alternative to PM machines associated with a controlled rectifier. When HE generators are operating in a local grid, the excitation flux can be used to control the terminal voltage level. Some of the advantages of HE machines are that the mass and size of the rotor poles can be kept low compared to overall designs that only use field windings, as the field windings and their cooling system can be decreased.

The aim of this paper is to study a new rotor design dedicated to the Electric Controlled Permanent Magnet Synchronous machine (ECPMS-machine) that uses two axially separated consequent poles, described in detail in [13–18]. The machine has, in addition to magnets embedded in the rotor, a field winding (FW) generating the magnetic field by a DC coil fixed on the stator. In the machine, each pole pair consists of one PM magnetized pole (PM pole) and one iron pole (iron pole) – that is an iron flux path. The iron poles without PMs are used as an advantage in hybrid excitation and are made of highly permeable iron compared to the low permeability of PM materials, which allows variations in the flux from the DC coil. It is important to know that the iron poles are affected by both the permanent magnet flux and the FW flux. Hybrid excitation in consequent pole machines, using an inner rotor, has been studied by Tapia et al. [19, 20] and others [21–26]. A concept for the application of the ECPMSM machine in EV drive systems regarding a dedicated control algorithm has been presented in [27].

2. ECPMS-machine with new rotor structure concept

Figure 1 presents a 12-poles ECPMS-machine prototype with a new rotor geometry concept. The main data of the machine prototype are listed in Table 1.

The stator of the ECPMS-machine (Fig. 2) consists of two stator cores with independent armature windings. Between the stator cores there is a single stator DC coil which is placed inside a single stator toroid core.

The rotor (Fig. 3) consists of two rotor cores, a single toroid rotor core and a shaft. What is important here is that, the three groups of magnetic flux barriers in the rotor core lamination are used. A specific shape and location of magnetic barriers in the rotor core lamination, arranged as shown in Fig. 4, cause that the reluctance of the PM pole is high, hence, it is possible to control the flux from the FW passing through the iron pole in a very effective way.

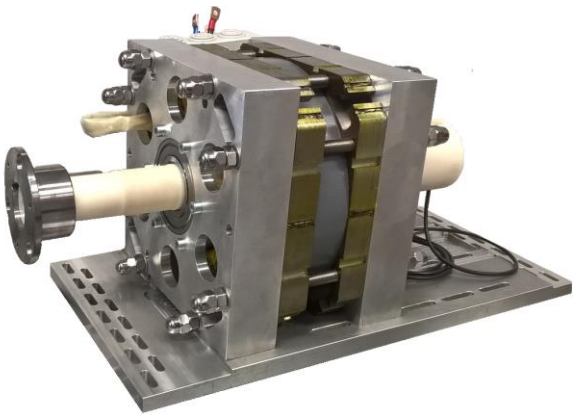

Fig. 1. Prototype of ECPMS-machine

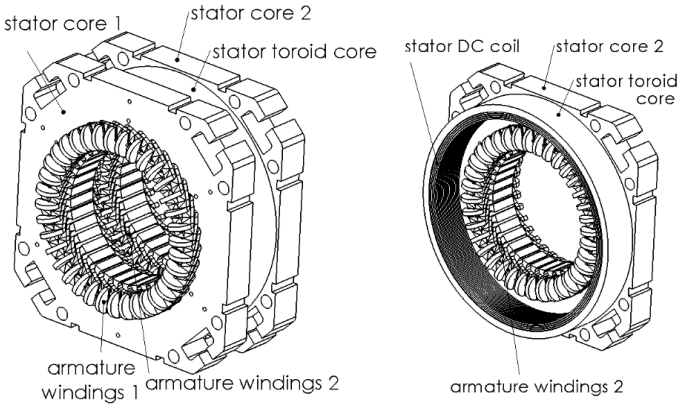

Fig. 2. Stator of ECPMS-machine

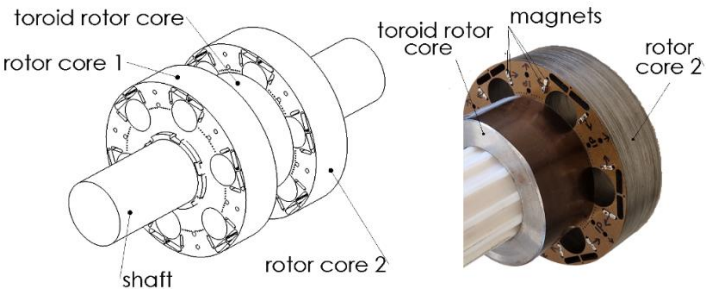

Fig. 3. A new rotor design concept for the ECPMS-machine

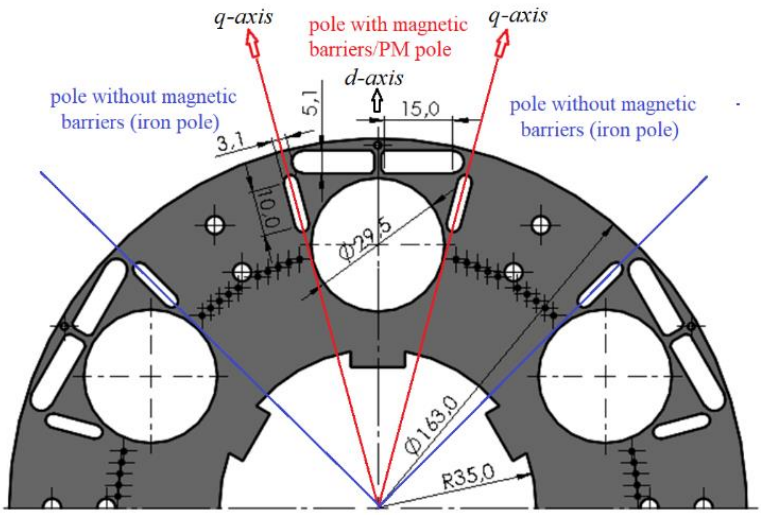

Fig. 4. A rotor core lamination with multi-flux barriers

Table 1. The main data of the machine prototype

Parameter name	**Value**	**Unit**
Number of poles	12	
Stator inner/outer diameter	164.0/326.0	mm
Stator axial length	2×40.0	mm
Number of slots	36	
Number of turns in slot	300	
Rotor outer diameter	163.0	mm
Rotor core axial length	2×40.0	mm
Toroid rotor core axial length	50.0	mm
Embedded PM grade/dimensions	$\mathrm{N35}/10 \times 3 \times 40$	mm
Air gap length	0.5	mm

3. The hybrid excitation flux and hybridization ratios

An electromotive force e of a multi-turn winding in HE machines is induced by the change in the hybrid excitation flux ϕ_{HE}, and is written as:

$$e = -k_w N \frac{\mathrm{d}\phi_{\mathrm{HE}}}{\mathrm{d}t} = -\frac{\mathrm{d}\psi}{\mathrm{d}t}, \tag{1}$$

where: k_w is the winding factor; N stands for turns of the winding; ϕ is the magnetic flux; ψ is the flux linkage.

The flux linkage ψ of the HE machine is the sum of the hybrid excitation flux ϕ_{HE}, and the flux of the armature magnetic reaction ϕ_a. In general, the hybrid excitation flux, ϕ_{HE} has two components: first, the permanent magnet flux linkage ϕ_{PM}; second, an additional excitation flux ϕ_{FW} excited by an FW, in this case, by the stator DC coil current I_{DC}. In the first simple approach, the combined flux can be written as:

$$\phi_{\mathrm{HE}} = \phi_{\mathrm{FW}}\,(I_{\mathrm{DC}}) + \phi_{\mathrm{PM}}. \tag{2}$$

The total flux path of the magnetic circuit and the reluctance of the iron depends on the flux density, where the flux ϕ_{FW} excited by the FW is controllable, since it is possible to control the hybrid flux ϕ_{HE} by controlling the magnetic field current I_{DC}. Except for the controllable flux, there is also another advantage of hybrid excitation, including the increased variety of machine designs that could be established when optimizing the hybridization. Therefore, it is necessary to determine the hybridization ratio, for example, as an optimization tool for design purposes. There are many publications [28–32] where the hybridization ratio was expressed.

During 3D-FE-analysis, three indicators of hybridization ratios denoted by α, β, γ were examined. The hybridization ratio α is defined as the ratio of the total excitation flux by the flux strengthening $\phi_{\mathrm{HE\_}s}$ to the no-load permanent magnets' flux linkage ϕ_{PM}:

$$\alpha = \frac{\phi_{\mathrm{HE\_}s}}{\phi_{\mathrm{PM}}}. \tag{3}$$

The hybridization ratio β is defined as the ratio of the total excitation flux by the flux weakening $\phi_{\mathrm{HE\_}w}$ to the permanent magnets flux linkage ϕ_{PM}:

$$\beta = \frac{\phi_{\mathrm{HE\_}w}}{\phi_{\mathrm{PM}}}. \tag{4}$$

The hybridization ratio γ is defined as the ratio of the total excitation flux by the flux strengthening $\phi_{\mathrm{HE\_}s}$ to the total excitation flux by the flux weakening $\phi_{\mathrm{HE\_}w}$:

$$\gamma = \frac{\phi_{\mathrm{HE\_}s}}{\phi_{\mathrm{HE\_}w}}. \tag{5}$$

These ratios could act as a way of analysing the operation and how the FW flux is operated compared to the flux excited by PMs, as well as for determining the flux density distribution and the machine performance for the different magnetic field current I_{DC}.

4. Magnetic field distribution

To show the effect of the change, no-load magnetic flux density distribution in the air-gap of the machine as a result of the additional excitation flux ϕ_{FW} exited by the FW, 3D FE- analyses have been carried out at the three different stator DC coil current I_{DC} loadings at 0 and ±5.0 ADC.

Figure 5(a) shows the magnetic field distribution in the 3D-FE-model of the ECPMS-machine with a base rotor structure, which was also used in the prototype of the machine. Figure 5(b) shows the vector field of magnetic flux density along the arc examined in the middle of the air gap of the machine with a rotor in case 1, at three different DC coil current loads.

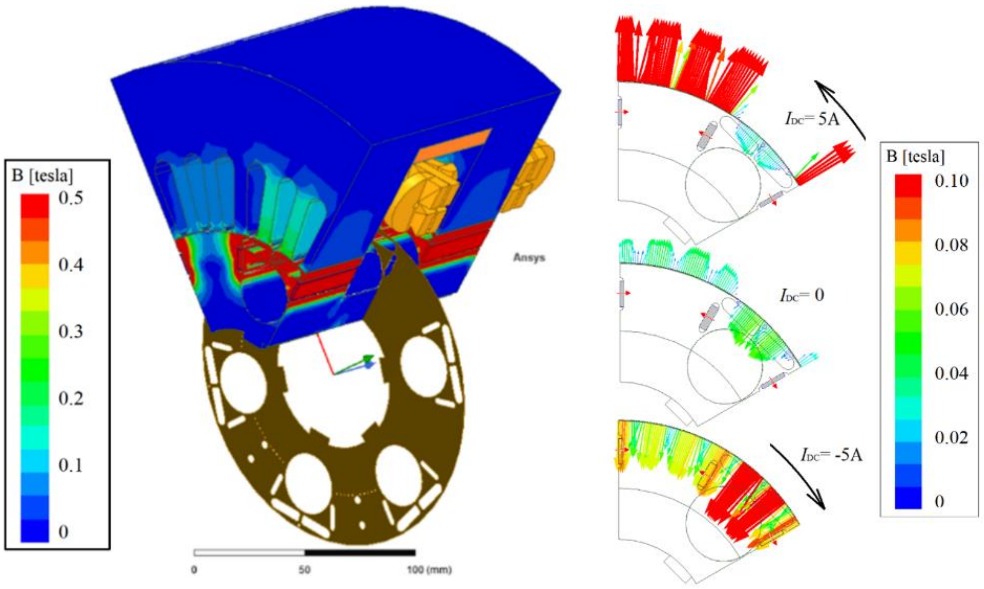

(a) (b)

Fig. 5. No-load magnetic field distribution in 3D-FE-model of ECPMS-machine with rotor (case 1) (a); vector field of magnetic flux density along the arc in the middle of the air gap at the three different DC current loads (0 and ±5.0 A) (b)

Figure 6 shows one pair of poles for the three study cases:

Case 1 – magnets (dimensions: $10.0 \times 3.0 \times 40.0$ mm) are inserted in radial magnetic flux barriers only (Fig. 6(a)).

Case 2 (add PM) – magnets (dimensions: $10.0 \times 3.0 \times 40.0$ mm) are inserted in radial magnetic flux barriers and additional magnets (dimensions: $5.0 \times 5.0 \times 40.0$ mm) are inserted in the main flux barriers (Fig. 6(b)).

Case 3 (add IC) – magnets (dimensions: $10.0 \times 3.0 \times 40.0$ mm) are inserted in radial magnetic flux barriers and additional iron components (IC) (dimensions: $10.0 \times 5.0 \times 40.0$ mm) are embedded in the main flux barriers (Fig. 6(c)).

The results show that the length change of the field vector in the middle of the air gap under the pole with main flux barriers is smallest while the additional excitation is increasing, compared to the length change of the field vector shown under the adjacent pole. Hence, it can be concluded that the proposed geometry of the rotor magnetic circuit effectively blocks an additional excitation flux passing through the pole with magnetic barriers. At the same time, the additional excitation flux passes through the adjacent pole successfully. Thanks to this, one can assume that it is possible to adjust the hybrid excitation flux ϕ_{HE} in an extensive range. In order to verify this assumption, additional theoretical investigations were performed.

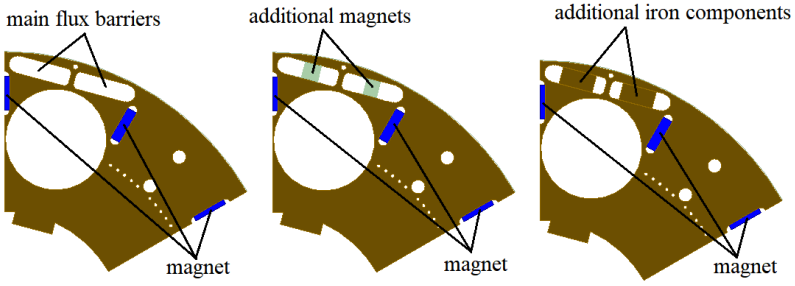

Fig. 6. Three cases of placing magnets and iron components in the rotor: Case 1 (a); Case 2 (b); Case 3 (c)

5. Flux linkage

A mathematical model of the machine has been developed under typical assumptions: armature windings are symmetric; windings' inductance and resistance, and permanent magnets' flux are constant; linearity of the magnetic circuit, as well as magnetic flux density higher harmonics, are neglected. Finally, the d- and q-axis voltages and the electromagnetic torque of the machine can be written as:

$$U_d = RI_d + \frac{\mathrm{d}\Psi_d}{\mathrm{d}t} - p\Omega_m\Psi_q, \tag{6}$$

$$U_q = RI_q + \frac{\mathrm{d}\Psi_q}{\mathrm{d}t} + p\Omega_m\Psi_d, \tag{7}$$

$$T_e = \frac{3}{2}p\left(I_q\Psi_d - I_d\Psi_q\right) = \frac{3}{2}p\left[\overbrace{\Psi_{\mathrm{pm}}I_q}^{T_{\mathrm{sync}}} + \overbrace{M_{\mathrm{DC}}I_{\mathrm{DC}}I_q}^{T_{\mathrm{DC}}} + \overbrace{\left(L_d - L_q\right)I_dI_q}^{T_{\mathrm{rel}}}\right], \tag{8}$$

where: p is the number of the pair poles; Ψ_d, Ψ_q represent the d- and q-axis magnetic fluxes; Ψ_{pm} is the flux generated by the PMs; I_d, I_q are the d- and q-axis stator currents; R is the resistance of the armature windings; L_d, L_q are the d- and q-axis inductances; M_{DC} stands for the mutual inductance of the additional stator coil; I_{DC} is the current in the stator DC coil.

Equation (8) shows the possibility of forming a specified electromagnetic torque at different values of the individual components of the stator current (I_d, I_q) and stator DC coil current I_{DC}.

Due to the additional degree of freedom in the form of resultant flux control by the DC coil current, it is possible to generate a torque setpoint at different values of stator current components I_d and I_q. If high torque is required at low speeds, the excitation flux can be increased, thus it is possible to reduce the armature current. At high rotational speeds, due to the induced high voltage, a current control strategy requires the weakening of the excitation flux. Reducing the flux can also affect the reduction of magnetic losses of the machine.

In order to account for the nonlinearity of the magnetic circuit, 3D-FE analysis was carried out to investigate the effect of DC coil currents on inductance and armature flux linkage. Figure 7 shows 3D-FEA results of d- and q-axis components of no-load inductance characteristics versus stator DC coil currents.

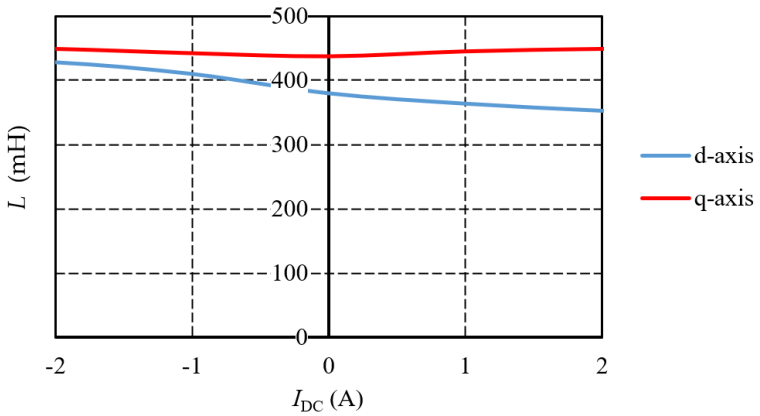

Fig. 7. No-load inductance versus stator DC coil currents characteristics

Figure 8 shows 3D-FEA results of d- and q-axis components of no-load armature flux linkage characteristics versus stator DC coil currents.

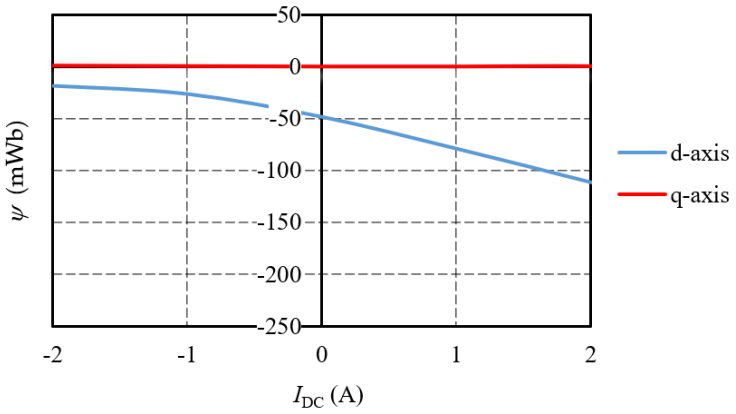

Fig. 8. No-load armature flux linkage versus stator DC coil currents characteristics

Figure 9 shows phase flux linkage waveforms achieved at the different DC current of the stator DC coil. In this case, the current loading of the stator DC coil was set in the range from −2.0 ADC to +2.0 ADC, which corresponds to the maximal value of magnetomotive force (MMF) equal to 600 Ampere-turns.

Figure 9 clearly shows a flux strengthening effect, which increases the value of armature flux linkage from 49.4 mWb to 112.4 mWb, while the stator DC coil current was changed from 0 to 2 A. Under the same current load conditions, changing the polarity of the current I_{DC}, a strong flux weakening effect can be observed, which results in a decrease in the value of armature flux linkage from 49.4 mWb to 18.0 mWb. Moreover, the achieved results show that under the stator DC coil loading at I_{DC} − 5.0 A, it is possible to change the polarity of the machine poles (Fig. 10) where the instantaneous (at 60 el. deg.) value of armature flux linkage has a negative value of 6.6 mWb.

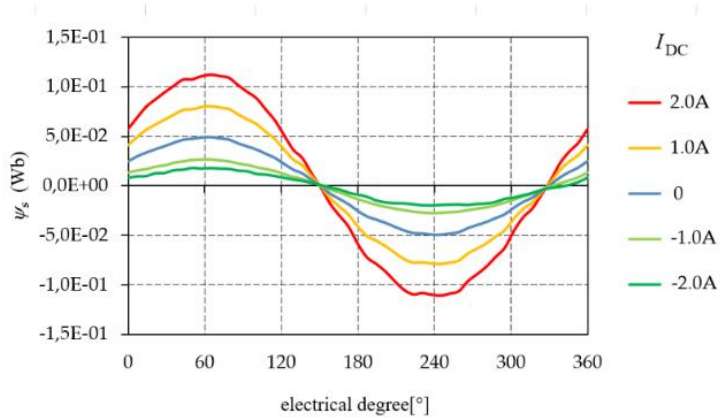

Fig. 9. No-load phase armature flux linkage waveforms at the different currents of the stator DC coil

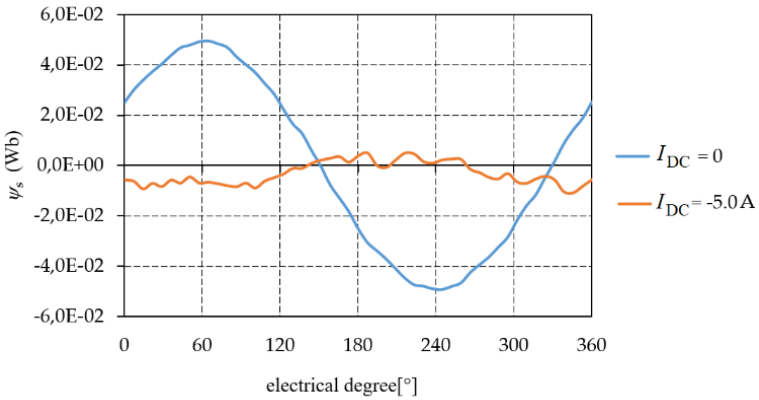

Fig. 10. No-load phase armature flux linkage waveforms at two currents of the stator DC coil $I_{DC} = 0$ and $I_{DC} = -5$ A

In order to confirm the effectiveness of varying the hybrid excitation flux ϕ_{HE}, an experiment was carried out on a machine prototype with a base rotor structure (case 1 experiment).

Figure 11 shows the measured line BEMF waveform at 1 000 rpm, at three different stator coil DC currents. In this case, the current loading of the stator DC coil was set to –1.0 ADC, 0 and +1.0 ADC, with +1.0 ADC corresponding to the value of MMF equal to 300 Ampere-turns.

Additionally, the rms value of line BEMF at 1 000 rpm rotor speed characteristic versus stator DC coil current was performed and shown in Fig. 12. Figure 13 shows cogging torque versus excitation field current I_{DC} characteristics.

The experimental results successfully confirmed 3D-FEA predictions. The results show that the rms value of line BEMF in strengthening mode at I_{DC} = 5.0 ADC equals 87.1 V, and it is four times greater than the voltage measured at I_{DC} = 0. It can be concluded that the proposed rotor geometry for the ECPMS-machine is worth attention. In this case it is possible to adjust the excitation flux of the machine in a very wide range. The results also show that the magnetic circuit of the machine is not saturated, even when the machine is fully excited by the stator DC coil.

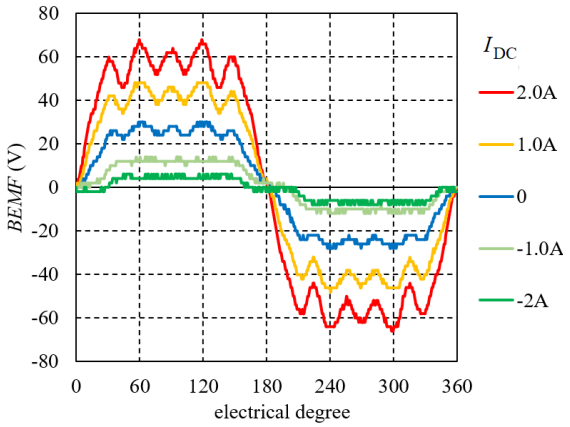

Fig. 11. Line BEMF waveforms measured at 1 000 rpm for three different stator coil DC currents

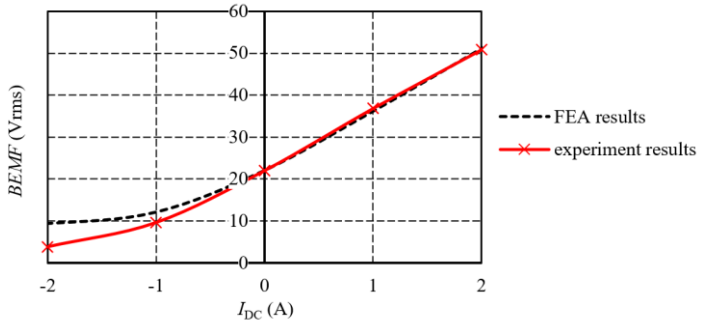

Fig. 12. Line BEMF characteristic versus DC coil currents (measured at 1 000 rpm)

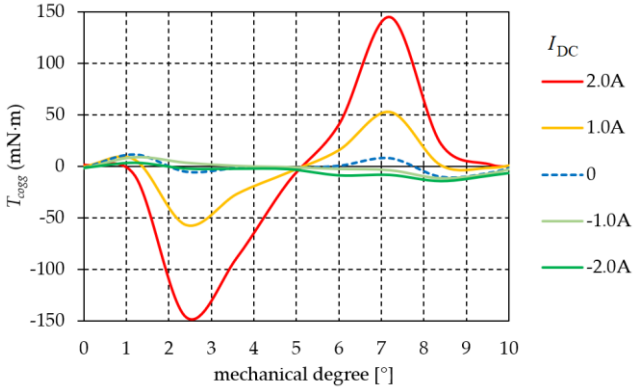

Fig. 13. Cogging torque vs. DC control coil currents

Hence, there is potential to increase the power density by introducing additional sources of the excitation flux (case 2) or changing the magnetic parameters by inserting additional ferromagnetic pieces into the main magnetic barriers (case 3).

The 3D-FE-analysis were performed for the other two cases. Figure 14 shows characteristics of no-load induced phase voltage in the stator windings obtained for all study cases of the additional DC coil current excitation. For these cases, the current loading of the stator DC coil was limited and set in the range from –2.0 ADC to +2.0 ADC (this corresponds to the value of MMF equal to 600 Ampere-turns).

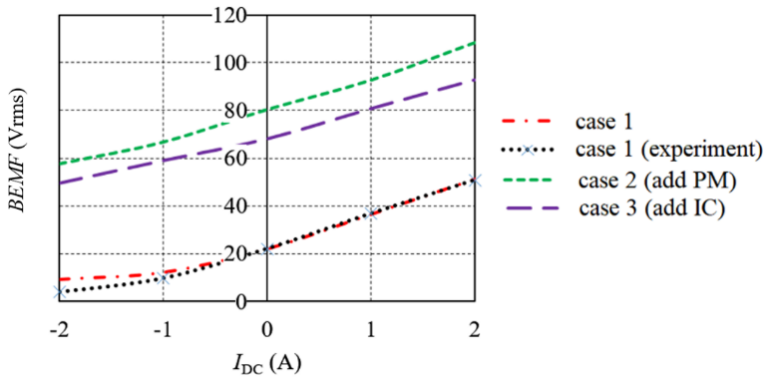

Fig. 14. Line BEMF characteristics versus stator DC coil current for all study cases

Based on the results, it can be concluded that the effect of additional magnets (case 2) and iron components (case 3) on the flux excitation control is significant. Table 2 summarizes the values of the back-emf versus stator coil current I_{DC} and hybridization rates α, β and γ for all study cases.

Table 2. Values of BEMF versus stator coil current and hybridization rates for all study cases

I_{DC}	Case 1	Case 1 experiment	Case 2	Case 3
–2 A	9.4 V	3.8 V	57.5 V	49.5 V
–1 A	12.3 V	9.6 V	66.6 V	59 V
0	22.1 V	22 V	80.2 V	68.1 V
1 A	36.5 V	36.8 V	92.5 V	80.8 V
2 A	51.2 V	50.8 V	108.2 V	92.9 V
α	2.3	2.3	1.3	1.4
β	2.4	5.7	1.4	1.4
γ	5.4	13.2	1.9	1.9

The presented results show that applying the additional magnets inside the magnetic barriers in the rotor structure increases the excitation flux by 360 percent; however, the total hybridization rate γ is reduced from 5.4 to 1.9. Adding the iron component by inserting it into the main magnetic barrier also increases the excitation flux by approx. 300 percent, and this time the total hybridization rate γ also falls to a similar level.

6. Conclusions

The purpose of this paper was to present a new rotor geometry concept with additional magnets and iron components in the rotor for the ECPMS-machine. The presented results show that the proposed rotor design for the machine may have a very good application potential to use the machine in variable speed drives. Based on the simulation results, it was observed that the effect of additional magnets and iron components in the presented rotor structure of the ECPMS-machine is significant. In general, it can be concluded that an appropriate selection of the width of the magnet and iron components allows one to obtain the required hybridization rate for the ECPMS-machine.

The further work will focus on studying magnet geometry to increase the power density of the machine while considering the expected hybridization rate, and reducing the induced back-emf pulsation, which is mainly unfavourable at low rotor speed regions.

References

[1] Amara Y., Hamid B.A., Gabsi M., *Hybrid Excited Synchronous Machines: Topologies, Design and Analysis*, John Wiley & Sons (2024).

[2] Hlioui S., Gabsi M., Ahmed H.B., Barakat G., Amara Y., Chabour F., Paulides J.J.H., *Hybrid excited synchronous machines*, IEEE Transactions on Magnetics, vol. 58, iss. 2, 8101610 (2022), DOI: 10.1109/TMAG.2021.3079228.

[3] Capolino G.-A., Cavagnino A., *New trends in electrical machines technology—Part II*, IEEE Trans. Ind. Electron., vol. 61, no. 9, pp. 4931–4936 (2014), DOI: 10.1109/TIE.2013.2295770.

[4] Zhu Z.Q., Cai S., *Hybrid excited permanent magnet machines for electric and hybrid electric vehicles*, CES Trans. Electr. Mach. Syst., vol. 3, no. 3, pp. 233–247 (2019), DOI: 10.30941/CES-TEMS.2019.00032.

[5] Asfirane S., Hlioui S., Amara Y., Gabsi M., *Study of a hybrid excitation synchronous machine: Modeling and experimental validation*, Math. Comput. Appl., vol. 24, no. 2, pp. 34 (2019), DOI: 10.3390/mca24020034.

[6] Wang Q., Niu S., Luo X., *A Novel Hybrid Dual-PM Machine Excited by AC with DC Bias for Electric Vehicle Propulsion*, IEEE Transactions on Industrial Electronics, vol. 64, iss. 9, pp. 6908−6919 (2017), DOI: 10.1109/TIE.2017.2682778.

[7] Hua H., Zhu Z.Q., Zhan H., *Novel Consequent-Pole Hybrid Excited Machine with Separated Excitation Stator*, IEEE Transactions on Industrial Electronics, vol. 63, iss. 8, pp. 4718–4728 (2016), DOI: 10.1109/TIE.2016.2559447.

[8] Afinowi I.A.A., Zhu Z.Q., Guan Y., Mipo J.C., Farah P., *Hybrid-Excited Doubly Salient Synchronous Machine with Permanent Magnets Between Adjacent Salient Stator Poles*, IEEE Transactions on Magnetics, vol. 51, no. 10, 8107909 (2015), DOI: 10.1109/TMAG.2015.2446951.

[9] Zepp L.P., Medlin J.W., *Brushless permanent magnet motor or alternator with variable axial rotor/stator alignment to increase speed capability*, AU2003217963A1 (2003).

[10] Tapia J.A., Leonardi F., Lipo T.A., *Consequent-Pole Permanent-Magnet Machine with Extended Field-Weakening Capability*, IEEE Trans. Ind. Appl., vol. 39, pp. 1704–1709 (2003), DOI: 10.1109/TIA.2003.818993.

[11] Kong L., Wen X., Fan T., *A new method to plan the optimal field excitation current trajectory in a hybrid excitation machine*, In Proceedings of the 2011 International Conference on Electrical Machines and Systems, Beijing, China, pp. 20–23 (2011), DOI: 10.1109/ICEMS.2011.6073691.

[12] Mörée G., Leijon M., *Overview of Hybrid Excitation in Electrical Machines*, Energies, vol. 15, no. 19, 7254 (2022), DOI: 10.3390/en15197254.

[13] Paplicki P., *Influence of Magnet and Flux-Barrier Arrangement on Flux Control Characteristics of Hybrid Excited ECPMS-machine*, Elektron. Elektrotech., vol. 23, pp. 15–20 (2017), DOI: 10.5755/j01.eie.23.2.14461.

[14] Wardach M., Paplicki P., Palka R., *Hybrid Excited Machine with Flux Barriers and Magnetic Bridges*, Energies, vol. 11, 676 (2018), DOI: 10.3390/en11030676.

[15] Di Barba P. *et al*., *Hybrid excited synchronous machine with flux control possibility*, International Journal of Applied Electromagnetics and Mechanics, vol. 52, no. 3–4, pp. 1615–1622 (2016), DOI: 10.3233/JAE-162190.

[16] Paplicki P., Prajzendanc P., Wardach M., Palka R., Cierzniewski K., Pstrokonski R., *Influence of Geometry of Iron Poles on the Cogging Torque of a Field Control Axial Flux Permanent Magnet Machine*, Int. J. Appl. Electromagn. Mech., vol. 69, pp. 179–188 (2022), DOI: 10.3233/JAE-210182.

[17] Prajzendanc P., Paplicki P., *Performance Evaluation of an Axial Flux Machine with a Hybrid Excitation Design*, Energies, vol. 15, 2733 (2022), DOI: 10.3390/en15082733.

[18] Wardach M., Palka R., Paplicki P., Prajzendanc P., Zarebski T., *Modern Hybrid Excited Electric Machines*, Energies, vol. 13, 5910 (2020), DOI: 10.3390/en13225910.

[19] Tapia J.A., Leonardi F., Lipo T.A., *Consequent pole permanent magnet machine with field weakening capability*, In Proceedings of the IEMDC 2001 IEEE International Electric Machines and Drives Conference, Cambridge, MA, USA, pp. 126–131 (2001).

[20] Tapia J.A., Leonardi F., Lipo T.A., *A design procedure for a PM machine with extended field weakening capability*, In Proceedings of the Conference Record of the 2002 IEEE Industry Applications Conference 37th IAS Annual Meeting Pittsburgh, PA, USA, vol. 3, pp. 1928–1935 (2002).

[21] Kosaka T., Matsui N., *Hybrid excitation machines with powdered iron core for electrical traction drive applications*, In Proceedings of the 2008 International Conference on Electrical Machines and Systems, Wuhan, China, pp. 2974–2979 (2008).

[22] Amemiya J., Chiba A., Dorrell D.G., Fukao T., *Basic characteristics of a consequent-pole-type bearingless motor*, IEEE Trans. Magn., vol. 41, pp. 82–89 (2005), DOI: 10.1109/TMAG.2004.840179.

[23] Asama J., Amada M., Takemoto M., Chiba A., Fukao T., Rahman A., *Voltage Characteristics of a Consequent-Pole Bearingless PM Motor with Concentrated Windings*, IEEE Trans. Magn., vol. 45, pp. 2823–2826 (2009), DOI: 10.1109/TMAG.2009.2018679.

[24] Asano Y., Mizuguchi A., Amada M., Asama J., Chiba A., Ooshima M., Takemoto M., Fukao T., Ichikawa O., Dorrell D.G., *Development of a Four-Axis Actively Controlled Consequent-Pole-Type Bearingless Motor*, IEEE Trans. Ind. Appl., vol. 45, pp. 1378–1386 (2009), DOI: 10.1109/TIA.2009.2023498.

[25] Ayub M., Jawad G., Kwon B.I., *Consequent-Pole Hybrid Excitation Brushless Wound Field Synchronous Machine with Fractional Slot Concentrated Winding*, IEEE Trans. Magn., vol. 55, no. 7, 8203805 (2019), DOI: 10.1109/TMAG.2018.2890509.

[26] Li J., Wang K., Zhu, S.S., Liu C., *Integrated-Induction-Based Hybrid Excitation Brushless DC Generator with Consequent-Pole Rotor*, IEEE Trans. Transp. Electrification, vol. 8, pp. 2233–2248 (2022), DOI: 10.1109/TTE.2021.3131307.

[27] Hlioui S., Gabsi M., Ahmed H.B., Barakat G., Amara Y., Chabour F., Paulides J.J.H., *Hybrid Excited Synchronous Machines*, IEEE Trans. Magn., vol. 58, iss. 2, 8101610 (2021), DOI: 10.1109/TMAG.2021.3079228.

[28] Paplicki P., Piotuch R., *Improved Control System of PM Machine with Extended Field Control Capability for EV Drive*, Mechatronics - Springer International Publishing, Ideas for Industrial Application, vol. 317, pp. 125–132 (2015), DOI: 10.1007/978-3-319-10990-9_12.

[29] Amara Y., Hlioui S., Ahmed H.B., Gabsi M., *Power Capability of Hybrid Excited Synchronous Motors in Variable Speed Drives Applications*, IEEE Trans. Magn., vol. 55, 8204312 (2019), DOI: 10.1109/TMAG.2019.2911599.

[30] Ammar A., Berbecea A.C., Gillon F., Brochet P., *Influence of the ratio of hybridization on the performances of synchronous generator with Hybrid Excitation*, In Proceedings of the 2012 XXth International Conference on Electrical Machines, Marseille, France, pp. 2921–2926 (2012).

[31] Amara Y., Hlioui S., Ben Ahmed H., Gabsi M., *Pre-optimization of hybridization ratio in hybrid excitation synchronous machines using electrical circuits modelling*, Math. Comput. Simul., vol. 184, pp. 118–136 (2020), DOI: 10.1016/j.matcom.2020.04.024.

[32] Shah Mohammadi A., Trovão J.P., Dubois M.R., *Hybridisation ratio for hybrid excitation synchronous motors in electric vehicles with enhanced performance*, IET Electr. Syst. Transp., vol. 8, no. 1, pp. 12–19 (2018), DOI: 10.1049/iet-est.2017.0029.